Memristive Circuit Implementation of Caenorhabditis Elegans Mechanism for Neuromorphic Computing

Hegan Chen, Qinghui Hong, Zhongrui Wang, Chunhua Wang, Xiangxiang Zeng, *Senior Member, IEEE*, and Jiliang Zhang, *Senior Member, IEEE*

***Abstract*— To overcome the energy efficiency bottleneck of the von Neumann architecture and scaling limit of silicon transistors, an emerging but promising solution is neuromorphic computing, a new computing paradigm inspired by how biological neural networks handle the massive amount of information in a parallel and efficient way. Recently, there is a surge of interest in the nematode worm Caenorhabditis elegans (C. elegans), an ideal model organism to probe the mechanisms of biological neural networks. In this article, we propose a neuron model for C. elegans with leaky integrate-and-fire (LIF) dynamics and adjustable integration time. We utilize these neurons to build the C. elegans neural network according to their neural physiology, which comprises: 1) sensory modules; 2) interneuron modules; and 3) motoneuron modules. Leveraging these block designs, we develop a serpentine robot system, which mimics the locomotion behavior of C. elegans upon external stimulus. Moreover, experimental results of C. elegans neurons presented in this article reveals the robustness (1% error w.r.t. 10% random noise) and flexibility of our design in term of parameter setting. The work paves the way for future intelligent systems by mimicking the C. elegans neural system.**

***Index Terms*— Caenorhabditis elegans, circuit design, memristor, neuromorphic computing, robot.**

I. Introduction

CONVENTIONAL computing with digital hardware faces great challenges to meet the ever-increasing demand for computing performance. On the one hand, this is because the von Neumann bottleneck, arising from the physically separated memory and processing units, inevitably yields massive and frequent data shuttling and large power/time consumption. On the other hand, transistor scaling, which has fueled the development of digital electronics, is dying [1], [2], [3]. Inspired by how the brain processes signals, neuromorphic computing is more parallel and efficient by emulating the structure and function of the human brain, such as asynchronous event-based parallelism and co-location of memory and computation. Furthermore, neurons, which can behave like synapses, may provide more efficient applicability of a neural network [4], [5].

Recent developments of neurorobotics, combining neuromorphic snake-like robots (NeuroSnake) and neurorobotic platform (NRP), focus on the improving efficiencies and capabilities of snake-like robots with a simplified brain model [6], [7], [8]. Snake-like robots feature snake-like gliding movements that are advantageous in complex and diverse environments, including earthquake sites, fire areas, and more [9], [10]. Such bionic robots are designed to imitate the structural characteristics and movement mechanisms of biological snakes. Its implementation plays a vital role in the development of neurorobotics [11], [12], [13].

Although the undulatory locomotion of snakes has been extensively studied [14], [15], it seems too complicated to unveil the mechanism from a cellular level due to the complexity of nervous systems and musculoskeletal structures. C. elegans is an ideal model to understand the locomotion mechanism, since its neural network is much simpler than other limbless animals, such as snakes [16], [17]. Specifically, C. elegans is one of the simplest and most well-investigated multicellular organisms, and its synaptic connections (approximately 8000) in neural networks have been investigated by electron microscope [18]. This small and simple nervous system of C. elegans exhibits surprisingly diversified behaviors, including learning, mating, foraging, and navigation [19], [20], [21].

Such undulatory locomotion is topical in the robotics field since it is the basis to design novel serpentine robots capable of traversing complex terrains [22], [23]. Karbowski et al. [24] used the biologically experimental results to constitute a neural network and illustrate how sinusoidal waves propagate through the body. Ren et al. [25] studied the morphology of C. elegans and designed a biomimetic crawling robot, which mimics the undulatory crawl of C. elegans using digital approximation. Furthermore, human-like robots are emerging. Jain et al. [26] researched humanoid bipedal robots with an

Manuscript received 23 April 2021; revised 12 May 2022 and 23 August 2022; accepted 23 February 2023. This work was supported in part by the National Natural Science Foundation of China under Grant 62001163, Grant 62234008, Grant 62122023, and Grant U20A20202; in part by the CCF-Huawei Populus Grove Fund under Grant CCF-HuaweiTC2022002; and in part by the Natural Science Foundation of Hunan Province, China, under Grant 2021JJ40111 and Grant 2020JJ4221. *(Corresponding author: Qinghui Hong.)*

Hegan Chen, Qinghui Hong, Chunhua Wang, Xiangxiang Zeng, and Jiliang Zhang are with the College of Computer Science and Electronic Engineering, Hunan University, Changsha 410082, China (e-mail: hongqinghui@hnu.edu.cn).

Zhongrui Wang is with the Department of Electrical and Electronic Engineering, The University of Hong Kong, Hong Kong 999077, China.

Color versions of one or more figures in this article are available at https://doi.org/10.1109/TNNLS.2023.3250655.

Digital Object Identifier 10.1109/TNNLS.2023.3250655

inertial measurement unit (IMU) to capture the robot locomotion of different lower extremity joints for human lower activities recognition. Moreover, his team calculated the joint angle of lower limbs of human gaits using Microsoft Kinect sensors and IMUs [27], [28]. So far, Karbowski et al. [24] and Ren et al. [25] focused on the physiology of C. elegans' neural networks, while Semwal et al. [52], [53] centered on the model of robot locomotion. A faithful bio-inspired system with optimal energy consumption and robustness is still yet to be demonstrated.

Most bionic circuit designs comprise capacitors, resistors, and complementary metal–oxide–semiconductor (CMOS) [29], [30]. However, these components have large circuit footprints and cannot cope with the requirements of high speed, high reliability, and low loss. Meanwhile, the limited on-chip learning abilities hinder the deployment of neuromorphic computing on real-world robots. In addition, CMOS-based neuromorphic computing is inefficient, where the efficiency of bionic robots is usually evaluated by the response speed in an unknown environment. In order to overcome those problems, we introduce a new circuit component, the memristor, which features a simple structure, a small footprint, low power consumption, easy integration, CMOS compatibility, and so on [31]. Memristors are circuit devices with built-in memory. Their memristance evolves with external voltages. This makes memristors share similar behaviors with the synapses of the human brain. As a result, memristors have been reported for wide applications in hardware neural networks [32], [33], [34], chaotic circuits [35], and so on.

In this article, we propose a memristive neuron circuit for C. elegans based on the LIF model, which integrates the inputs via synapses to produce action potentials. Its temporal reaction is determined by either the RC time constant of the integrator circuit or the state variables of memristors. Combining the C. elegans neuron model and the synaptic connections of C. elegans, we devise the memristive circuit that replicates the signal processing in C. elegans. Furthermore, the serpentine robot architecture based on modular design presented in this work mimics the locomotion mechanism of C. elegans under the control of the memristive neuromorphic system. In addition, we simulated the above-mentioned design with noise injection, which illustrates the strong robustness due to the feedback loop. Meanwhile, circuit parameters can be flexibly tuned according to different requirements. The memristive circuit and bio-inspired mechanism (C. elegans) endow the design with superior efficiency, parallelism, and robustness.

The rest of this article is organized as follows. Section II introduces the C. elegans touch-response mechanism and the C. elegans network model. Section III details the three components of the C. elegans circuit, including the sensory neuron module, interneuron module, and motoneuron module. Section IV illustrates the entire bionic circuit design and its simulation results in detail. Section V proposes the serpentine robot architecture based on the modular design. Section VI presents the conclusions and future work. All the circuit simulations were run in PSpice.

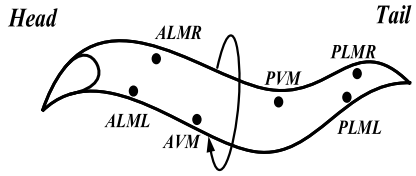

Fig. 1. Distribution map of C. elegans sensory neurons.

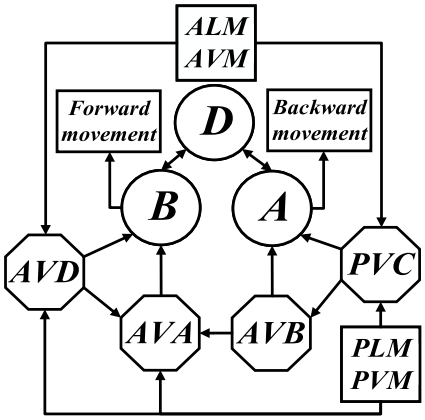

Fig. 2. Schematic of C. elegans locomotion-related network.

II. Locomotion-Related Biological Networks and Mathematical Model of C. elegans

Chalfie et al. [36], [37], [38] used laser ablation technology, isotope tracking, and other biological experimental methods to research the electrophysiological characteristics of the C. elegans neural network which focused on the functional properties of C. elegans neural network and related specific neurons that regulate contact-sensing motor and synapses. This section introduces in detail the C. elegans neural network for forward and backward locomotion.

A. Composition of C. elegans Locomotion-Related Network

According to the function of neurons, they are divided into three major categories: sensory neurons, interneuron, and motoneurons. C. elegans perceives the surrounding environment via some touch receptor neurons (TRNs) [39], [40]. As shown in Fig. 1, there are anterior lateral microtubule (ALM) (R/L) and anterior ventral microtubule (AVM) in the anterior half of the body, and posterior lateral microtubule (PLM) (R/L) and posterior ventral microtubule (PVM) in the posterior body. In particular, AVM and PVM are less sensitive than ALM and PVM [41], [42]. Body-wall muscle is divided into four quadrants (see Fig. 1) termed ventral-right (VR), dorsal-right (DR), ventral-left (VL), and dorsal-left (DL) quadrants, respectively. When C. elegans is stimulated to crawl, it uses the left or right body-wall muscle to touch the ground and crawls over a surface by propagating the dorsal/ventral flexures.

The middle layer is composed of interneurons AVD, AVA, AVB, and PVC, as shown in Fig. 2. It receives the signals from the sensory neuron and converts that to commands to downstream motoneurons. In addition, there are three kinds of motoneuron in C. elegans, including motoneuron A, B, and D. Motoneuron A promotes the backward movement of

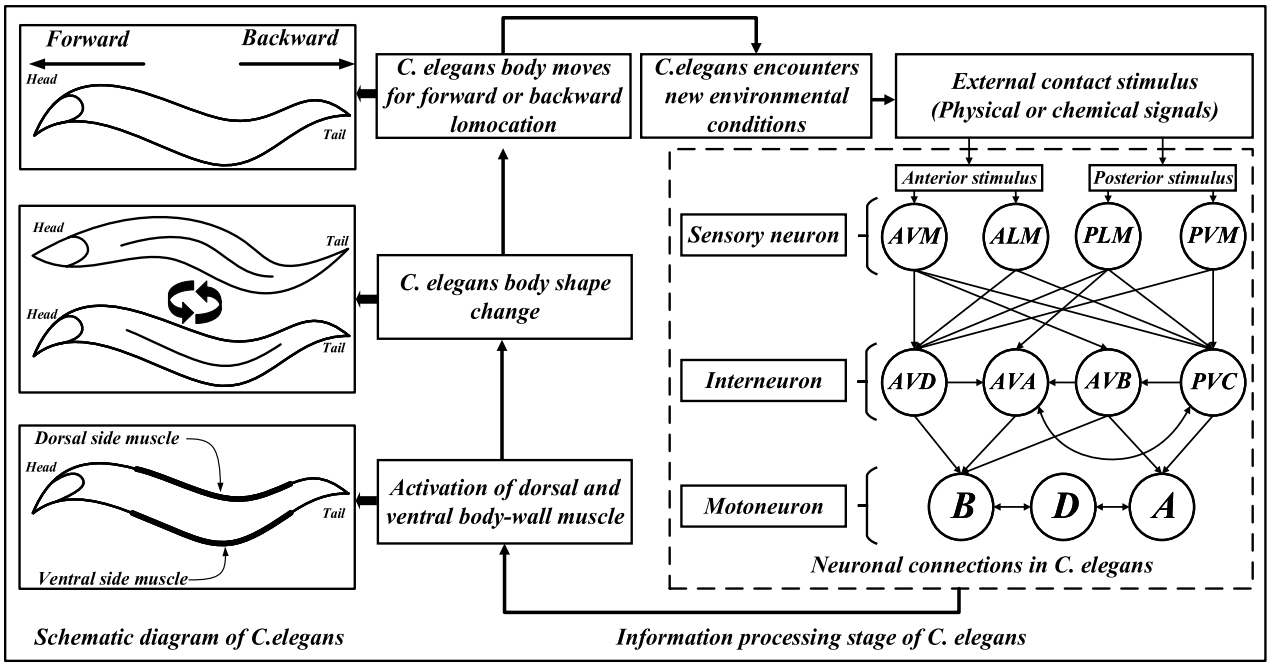

Fig. 3. Component of neural network of C. elegans and the stages of information processing when C. elegans encounters new environmental conditions.

C. elegans, while motoneuron B promotes forward movement. Motoneuron D receives signals from motoneuron A and B, which is not directly connected to interneurons. Motoneuron D could inhibit C. elegans muscle contraction via feedback mechanism.

B. Biological Mechanism of C. elegans Touch Response

As shown in Fig. 3, C. elegans can detect and react to chemotaxis, thermotaxis, and oxygenation. At first, C. elegans receives stimulus in a new environment. There are several kinds of mechanical stimuli like a head gentle touch, head heavy touch, tail gentle touch, and tail heavy touch. Body gentle touch, anterior or posterior stimulus, is a type of mechanical stimulation occurring frequently on C. elegans. Our work focuses on the effects of gentle touch on the anterior or posterior region of C. elegans.

When gentle anterior touch is applied to the C. elegans, sensory neurons (AVM and ALM) located in the anterior body are activated. Then, AVM and ALM excite the interneurons AVD and AVA while inhibiting interneurons PVC and AVB. Furthermore, motoneuron A gets excited which results in posterior movements. Similarly, the complementary series of locomotion takes place when posterior touch is applied (tail is gently touched). C. elegans utilizes dorsal and ventral flexure of body-wall muscle to crawl, and the muscle flexure is determined by A and B motoneuron. Once A or B motoneuron gets excited, it signals to contract and relax the body-wall muscle. Based on the above-mentioned discussion, C. elegans can change shape to exploit roughness in the terrain for forward or backward locomotion. When C. elegans encounters new environmental conditions, its sensory neurons perceive new stimuli and then C. elegans generate new movements.

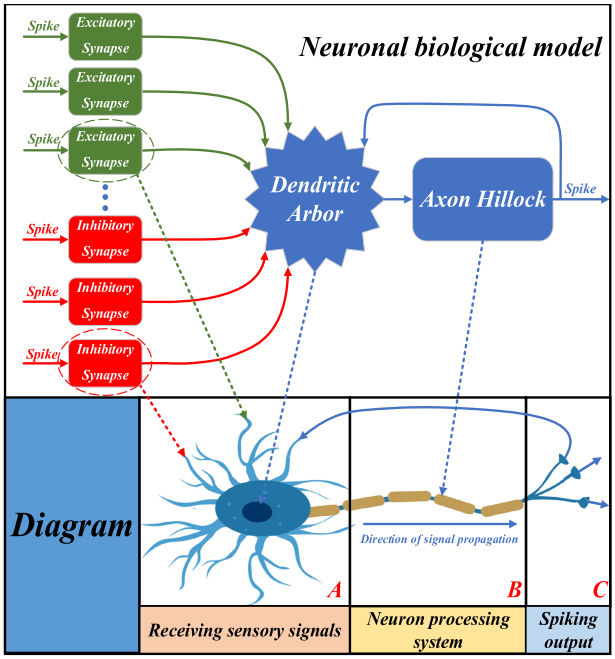

Fig. 4. Block diagram of neuron model. Part A is used for receiving sensory signals from different synapses, which include two kinds of inputs: excitatory and inhibitory. Part B is neuron processing system, which processes sensory signals nonlinearly. The function of part C is to output spiking signals.

C. elegans Neuron Model

The fundamental neuron model [43], [44] is composed of parts, including inhibitory synapses, excitatory synapses, dendritic arbor, and axon hillock, as shown in Fig. 4. When a presynaptic neuron spikes, the synapse generates a postsynaptic potential (PSP) whose property (positive or negative) depends on the polarity of the synapse (excitatory

or inhibitory). The entire PSPs, which come from different synapses (part A), are responsible for the growth of potential in dendritic arbor via a series of nonlinear operations (part B). For spiking neurons (part C), the axon hillock is likely to spike once the sum of accumulated potential exceeds the threshold. The biological model of C. elegans neuron could be defined in the following way:

$$\begin{cases} f(\theta(t)) = V_{\text{spike}}(t) \\ \theta(t) = \sum_{j=1}^{m} \alpha_j \times V_{sj}(t) + V_{\text{spike}}(t) \end{cases} \tag{1}$$

where $V_{\text{spike}}(t)$ represents the impulse output voltage of the neuron, α_j is the weight of j_{th} neuron, $V_{sj}(t)$ $(j = 1, 2, 3, \ldots, m)$ is the neuron input j_{th}, and $\theta(t)$ represents the sum of all inputs of neurons and $V_{\text{spike}}(t)$, $f(\theta(t))$ is the function of axon hillock which can be set as a requirement.

III. Memristive Bionic Circuit Design of C. elegans Biological Network

The memristive circuit design of C. elegans mainly simulates the movement of C. elegans after receiving stimulation. The circuit consists of three parts: 1) the sensory neuron module. 2) The interneuron module. 3) The motoneuron module.

A voltage-controlled threshold memristor synapse (MS) model is used in this work [45]. If the input is a positive (negative) pulse voltage, the memristance decreases (increases) quickly and slowly decreases (increases) at the end of the transition. The derivative of the state variable for an MS memristor is

$$\frac{\mathrm{d}w(\mathrm{t})}{dt} = \begin{cases} \mu_v \dfrac{R_{\text{ON}}}{D} \dfrac{i_{\text{off}}}{i(t) - i_0} f(w(\mathrm{t})), & v(t) > V_{\text{TH+}} > 0 \\ 0, & V_{T-} \le v(t) \le V_{T+} \\ \mu_v \dfrac{R_{\text{ON}}}{D} \dfrac{i_{(t)}}{i_{\text{on}}} f(w(\mathrm{t})), & v(t) < V_{\text{TH-}} < 0 \end{cases} \tag{2}$$

$$f(\omega(t)) = 1 - \left(\frac{2w(t)}{D} - 1\right)^{2p} \tag{3}$$

$$v(t) = \left(R_{\text{off}} - \frac{w(t)}{D}\Delta R\right) \cdot i(t) \tag{4}$$

where D, i_0, i_{off}, and i_{on} are constants. v(t) is the applied voltage of the memristor, μ_v is the average ion mobility, ω(t) is the width of the doped region, $V_{\text{TH+}}$ and $V_{\text{TH-}}$ are the positive and negative threshold voltages, respectively, f(w(t)) is a window function, p is a positive integer, and R_{ON} and R_{OFF} are the lowest memristance and highest memristance of the memristor, respectively. The parameters of the MS used in the sensory, interneuron and motoneuron modules, and C. elegans network circuit are listed in Table I.

A. Memristive Circuit Design of C. elegans Neuron Model

In this article, we propose the memristive circuit design of C. elegans neuron model inspired by the LIF model [46], [47]. The following formula define the newly developed C. elegans neuron model, which is a modification of LIF neuron model:

$$R_i C_i \frac{dV_i(t)}{dt} = \frac{R_{Ci}}{M_{Ci}} \times \sum_{j=1}^{m} \alpha_{ij} \times V_j(t) - V_i(t) \tag{5}$$

where $V_i(t)$ is the membrane potential of a neuron i_{th}, $V_j(t)$ is the voltage input of neuron j_{th}, R and C are the parameters of the integrator determining time constant, t is the time, R_{Ci} and M_{Ci} are the two resistances of the inverting amplifier in the neuron i_{th}.

Suppose that an interneuron has a total of the n neuron inputs, α_{ij} $(i = 1, 2, 3, \ldots, n;\ j = 1, 2, 3, \ldots, m)$ is the connection weight of the j_{th} input neuron, which can be described with the following matrix:

$$R_i \times \begin{pmatrix} \frac{1}{R_{11}} & \frac{1}{R_{12}} & \frac{1}{R_{13}} & \cdots & \frac{1}{R_{1m}} \\ \frac{1}{R_{21}} & \frac{1}{R_{22}} & \frac{1}{R_{23}} & \cdots & \frac{1}{R_{2m}} \\ \frac{1}{R_{31}} & \frac{1}{R_{32}} & \frac{1}{R_{33}} & \cdots & \frac{1}{R_{3m}} \\ \vdots & \vdots & \vdots & \ddots & \vdots \\ \frac{1}{R_{n1}} & \frac{1}{R_{n2}} & \frac{1}{R_{n3}} & \cdots & \frac{1}{R_{nm}} \end{pmatrix}. \tag{6}$$

The corresponding circuit design is given in Fig. 5, which composes of an arbitrary number of inputs. When the sum of voltage passing through the adder exceeds the threshold of the memristor M_{ci}, M_{ci} immediately decreases, resulting in a

TABLE I
Parameters of MS Memristor

Parameters of MS	*Setting1*[1]	*Setting2*[2]	*Setting3*[3]
$R_{ON}(k\Omega)$	10	10	0.5
$R_{OFF}(k\Omega)$	20	40	100
$V_{TH+}(V)$	+0.0001	+0.04	+0.0001
$V_{TH-}(V))$	−0.02	−0.04	−0.0001
$D(nm)$	3	3	3
$u_v(m^2 s^{-1}\Omega^{-1})$	2.0×10^{-14}	2.0×10^{-14}	2.0×10^{-14}
$i_{on}(A)$	5.1×10^{-7}	5.1×10^{-7}	5.1×10^{-7}
$i_{off}(A)$	1.0×10^{-5}	1.0×10^{-5}	1.0×10^{-5}
p	10	10	10

[1] Parameters in Setting1 are used in M_s, M_{AVM}, M_{ALM}, M_{PLM} and M_{PVM}.
[2] Parameters in Setting2 are used in M_{AVD}, M_{AVA}, M_{AVB} and M_{PVC}.
[3] Parameters in Setting3 are used in $M_{Ai}(i = 1, 2, 3)$, M_A and M_B.

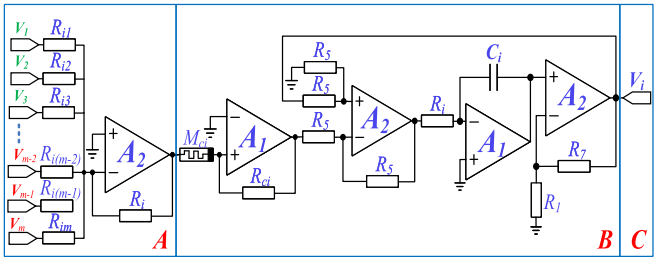

Fig. 5. Memristive circuit schematic of C. elegans neuron. In part A, input signals V_j $(j = 1, 2, 3, \ldots, m;)$ are summed by respective weights through the adder. In part B, the feedback amplifier circuit can integrate and amplify the sensory signals. M_{ci} memristor is used to balance voltage and prevent the excessive sum of sensory signals. Part C is the output port of C. elegans neuron.

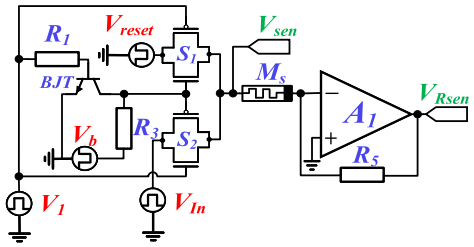

Fig. 6. Memristive circuit schematic of sensory neuron module includes three inputs, V_1, V_{In}, and V_{reset}.

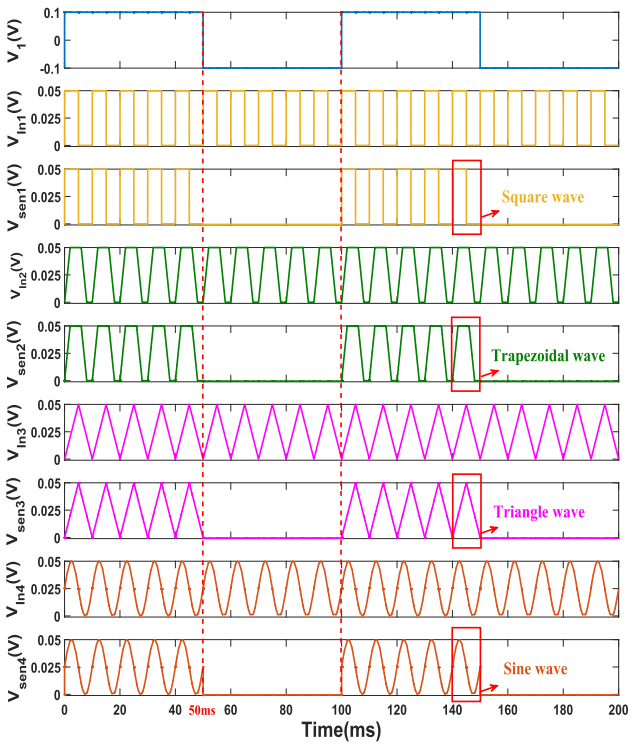

Fig. 7. Simulation results V_{Sen} of sensory module by receiving sensory signals with different shapes. The amplitudes and duty cycles of V_{Ini} $(i = 1, 2, 3, 4)$ is 0.05 V and 50%, respectively. The shapes of input sensory signals are square wave, trapezoidal wave, sine, and triangle wave, respectively.

decrease in the gain of the inverting amplifier. The proposed circuit contains an autonomous excitation part to oscillate itself. The voltage of the inverting amplifier, through the subsequent subtractor, integrator, and noninverting amplifier, achieves negative feedback.

B. Memristive Circuit Design of Sensory Neuron Module

The sensory neuron module is shown in Fig. 6, and its parameters could be tuned according to different requirements. The module consists of two switches (S_1 and S_2), two inverting amplifiers, and a memristor, and the model for sensory neuron behaves as

$$V_{\text{Sen}} = \begin{cases} V_{\text{In}} & V_1 > 0 \\ V_{\text{reset}} & \text{else}, \end{cases} \tag{7}$$

$$V_{\text{Rsen}} = \begin{cases} \dfrac{R_1}{M_s} \times V_{\text{In}} & V_1 > 0 \\ \dfrac{R_1}{M_s} \times V_{\text{reset}} & \text{else} \end{cases} \tag{8}$$

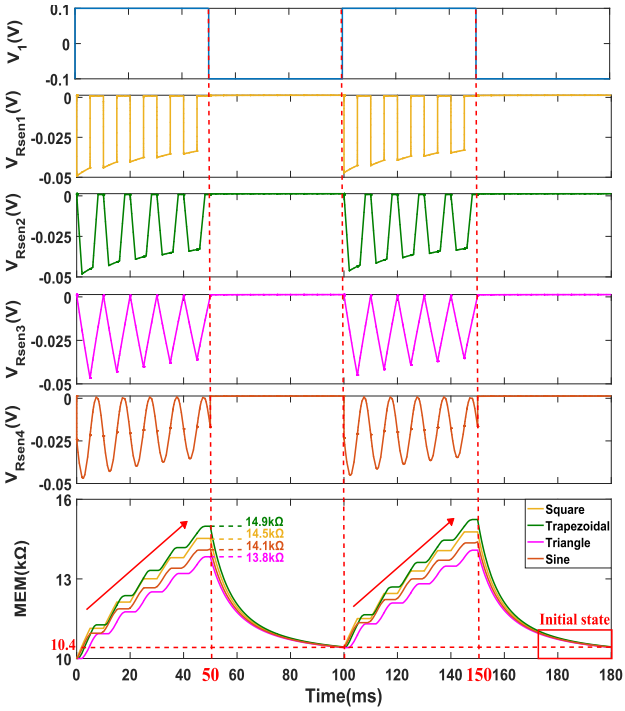

Fig. 8. Simulation results V_{Rsen} of sensory module by receiving sensory signals with different shapes. The amplitudes and duty cycles of $V_{\text{Ini}}(i = 1, 2, 3, 4)$ is 0.05 V and 50%, respectively. The shapes of input sensory signals are square wave, trapezoidal wave, sine wave, and triangle wave, respectively.

where V_1 is the stimulus (control signals), V_{In} is the oscillation wave of sensory neurons, and (R_1/M_s) represents the gain of the inverting amplifiers. It should be noted that V_{Sen} and V_{Rsen} represents the excitatory and inhibitory effect, respectively. If V_1 is above 0, the sensory neuron module receives sensory signals and propagates V_{In} to the interneuron module. Especially, S_2 is on and S_1 is closed, so V_{In} propagates to the output. Otherwise, S_2 is closed and S_1 is on, reset voltage (V_{reset} is an extremely small voltage of about 0 V) is applied to the memristor.

Simulation results of the sensory neuron module are shown in Figs. 7 and 8. The oscillation waves $V_{\text{Ini}}(i = 1, 2, 3, 4)$ have the same amplitude (0.05 V), period (200 ms), and duty cycle (50%), but different shapes. When V_{Ini} is greater than the threshold of M_{si}, M_{si} increases and V_{Rseni} tends to decrease. After the stimulus disappears, M_{si} basically returns to the initial state (LRS). It is noted that different shapes of oscillation waves with the same parameters affect the variation of the memristance. Simulation results (see Fig. 8) indicate that memristance changes rapidly in case of applying the trapezoidal wave, the memristance changes slowly in the case of applying the triangle wave. Therefore, it can be found that the response time is the shortest when the trapezoidal wave is applied, and the response time is the longest when a triangle wave is applied. In the following simulation, this article adopts the square wave as the waveform of the input signal.

C. Memristive Circuit Design of Interneuron Module

This section takes the interneuron AVD as an example to illustrate the mathematical model and internal logic of interneurons.

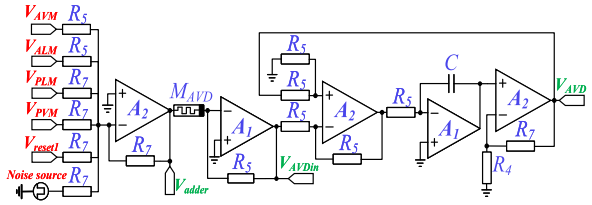

Fig. 9. Memristive circuit schematic of interneuron AVD module as an example.

The circuit of the AVD module is shown in Fig. 9. Its feedback amplifier circuit includes a basic amplifier circuit and a feedback network. Since the feedback network forms a closed loop, V_{AVD} is both the output signal and the feedback signal. The basic amplifier consists of subtractors, integrators, a memristor, and noninverting amplifiers, and the model of interneuron AVD is described as

$$\begin{cases} R_3 C \dfrac{d(V_{\mathrm{AVD}})}{\mathrm{dt}} = \omega_{\mathrm{AVD}} \times V_{\mathrm{AVD}} - \tau_{\mathrm{AVD}} \times V_{\mathrm{AVDin}} \\ V_{\mathrm{AVDin}} = \dfrac{R_1}{M_{\mathrm{AVD}}} \times (V_{\mathrm{AVM}} + V_{\mathrm{ALM}} + V_{\mathrm{PLM}} \\ +V_{\mathrm{PVM}} + V_{\mathrm{reset1}}) \end{cases} \tag{9}$$

where ω_{AVD} and (R_1/M_{AVD}) are the gain of the basic amplifying circuit and the inverting amplifiers, respectively. R_1 and M_{AVD} are the constant resistance and the memristor in AVD, respectively. To make it easier to understand, V_{AVDin} is described as an intermediate variable to represent the overall effect of input signals.

Simulation results of the AVD module are shown in Fig. 10. Before 45 ms, the constant accumulation of the input signals exceeds the threshold of M_{AVD}, and thus, M_{AVD} increases gradually but remains unchanged when input signals are 0 V. Meanwhile, V_{AVDin} decrease at the rate of the gain (R_1/M_{AVD}), meanwhile, (R_1/M_{AVD}) is dropping constantly. At 45 ms, V_{AVD} reaches a peak (36 mV) and then declines. Between 70 and 72 ms, reset voltage V_{reset1} plays a role of resetting M_{AVD} to initial state (11.9 kΩ). After the second input signal state (100 – 145 ms), V_{VAD} reaches the peak (43 mV), which is above the last one due to the accumulated effect of voltage.

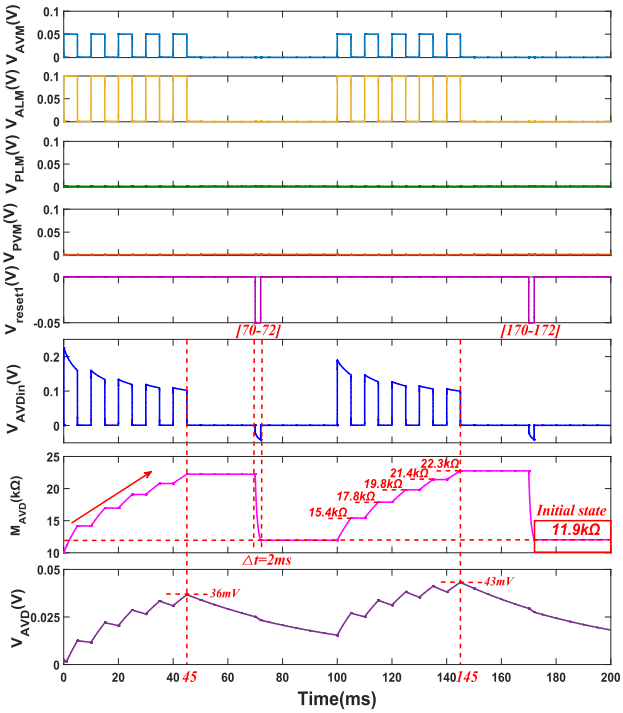

Fig. 10. Simulation results of interneuron AVD module when C. elegans receive anterior stimulus. The amplitudes of V_{AVM} and V_{ALM} are 0.05 and 0.1 V, respectively, as well as the same duty cycles (50%). The amplitudes of V_{PLM} and V_{PVM} maintain 0 V, which is regarded as not receiving the posterior stimulus.

D. Memristive Circuit Design of Motoneuron Module

This section takes the motoneuron A (see Fig. 11) as an example to depict the mathematical model and internal logic of the motoneuron. The structure of motoneuron modules is similar to interneuron modules; furthermore, the motoneuron module has an extra spiking module. Specifically, the spiking module selects a waveband, which exceeds the threshold of the memristor and generates a spiking pulse. The circuit calculation expression of motoneuron A is as follows:

$$R_3 C \frac{d(V_A)}{dt} = \tau_A \times (V_{\mathrm{AVD}} + V_{\mathrm{AVA}} + V_{\mathrm{AVB}} + V_D) - \omega_A \times V_A \tag{10}$$

$$V_{\mathrm{Apin}} = \frac{R_1}{M_A} \times (V_2 - V_A) \tag{11}$$

$$V_{Ap} = \begin{cases} 1 & V_{\mathrm{Apin}} > 0 \\ 0 & \text{else} \end{cases} \tag{12}$$

where ω_A and (R_1/M_A) are the gain of the basic amplifying circuit and the inverting amplifiers, respectively. R_1 and M_A are the constant resistance and the memristor in A, respectively. To make it easier to understand, V_{Apin} is described as an intermediate variable of internal logic in the circuit. Meanwhile, V_{Apin} indicates the selected waveband to be amplified with the help of the inverted amplifier.

Simulation results of the motoneuron. A module is shown in Fig. 12. At about 60 ms, V_A reaches its first peak (35 mV) but is below the threshold of M_A (38 mV). As input signals gradually increase, V_A first rises before decreasing to 0 V. At point A (144 ms), V_A exceeds the M_A's threshold, and thus, M_A declines dramatically from 100 kΩ at the point C. The time of V_A to exceed the threshold is Δt_2 (6 ms), where the maximum voltage reaches 41 mV. Zero cross detector plays an important role in outputting spiking pulse during the Δt_3. After 171 ms, V_A is below 38 mV, M_A returns to initial state (100 kΩ).

The main function of motoneuron D is to inhibit the contraction of C. elegans muscles via a feedback mechanism, in order to balance the locomotion of C. elegans function. The model of motoneuron D could be defined in the following way:

$$\frac{d(V_D)}{dt} = \frac{(V_A + V_B)}{\tau_D} - \omega_D \times V_D. \tag{13}$$

E. Noise Analysis of Interneuron Module

To validate the robustness of bionic circuit design, we have modeled the variability and nonidentities of transistors, resistors, and memristors [48], aiming to examine their impact on mimicking the locomotion of C. elegans. Specifically,

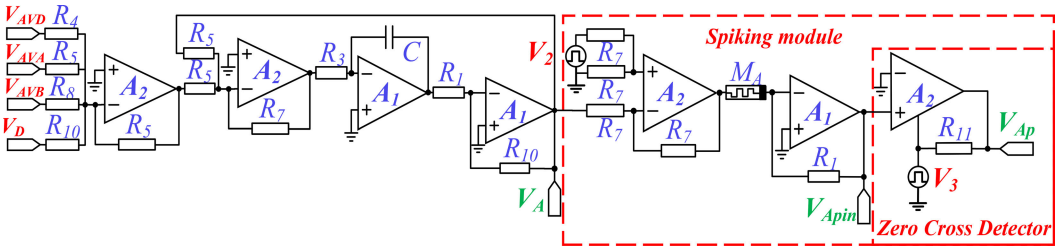

Fig. 11. Memristive circuit schematic of motoneuron A module as an example.

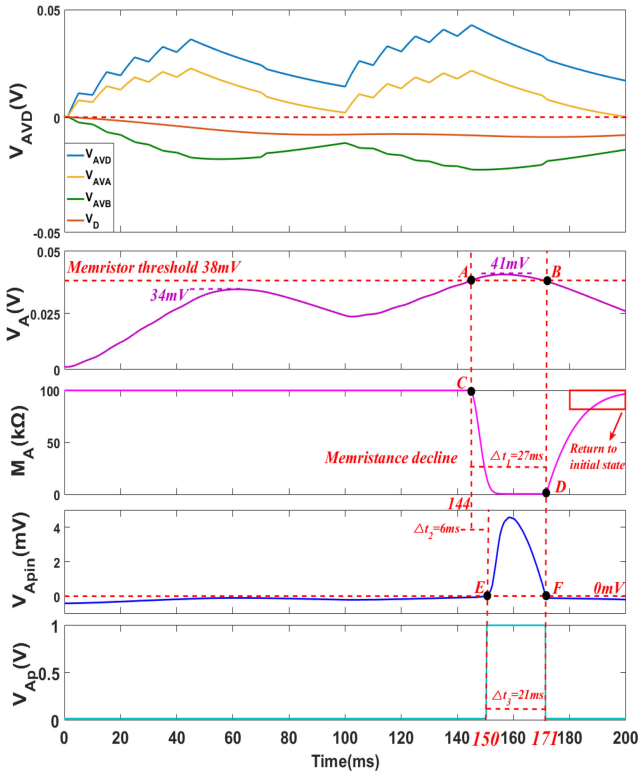

Fig. 12. Simulation results of motoneuron A module when C. elegans receive anterior stimulus. The module includes four input signals V_{AVD}, V_{AVA}, V_{AVB}, and V_D.

noise, such as voltage and current noise of the amplifier and the thermal noise of resistors, results in the variability of circuit components, which affects the performance of our design. In order to test the effect of noise, we simulate the interneuron AVD module by adding different levels of noise (5%, 10%, 15%, and 20%) to the input of the adder in AVD. Fig. 13 shows that the noise injections with different values affect the sum of the adder and final output of AVD in a limited way. With such noise injection, circuit error is described by the following equation:

$$Error(j) = \eta_e \times \frac{\sum_{i=1}^{n} abs\left(V_i^s - V_i^j\right)}{n}. \tag{14}$$

Here, V^s and V^j are the circuit outputs without noise and with jth level noise input, respectively. η_e is equal to $(V^s_{\min}/V^s_{\max})$ and n is the total of time steps between 200 ms.

Thus, Fig. 14 shows that our module is highly resilient to noise below 20%. The maximum variation is about 0.1% and the mean error is changed by 1.5%, which shows that our circuit can withstand 0%–20% variation of resistors without significant degradation in performance.

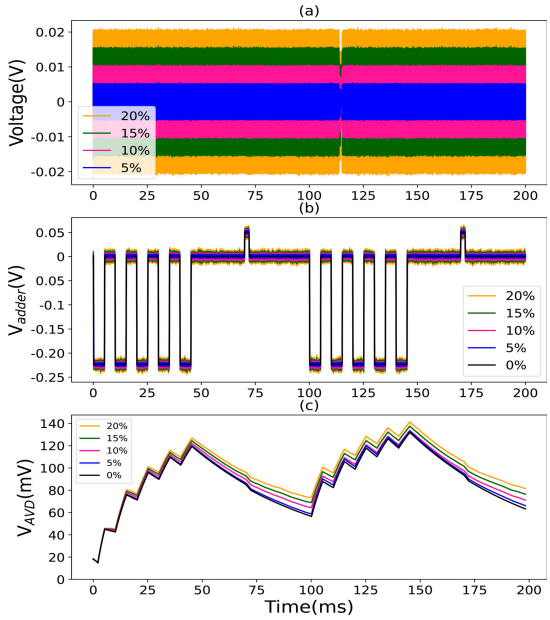

Fig. 13. Noise of interneuron AVD module and its effect on the bionic performance. (a) Gaussian noise sources in different standard deviations. (b) Output of Adder in the AVD module. (c) Output of interneuron AVD module.

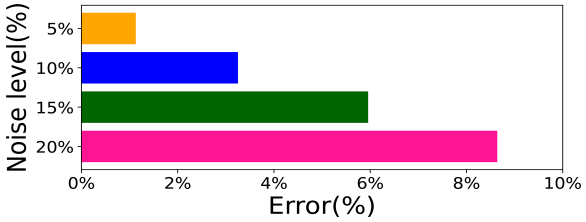

Fig. 14. Error of interneuron AVD module in the different noise level.

TABLE II
PARAMETERS OF THE MEMRISTIVE BIONIC C. ELEGANS CIRCUIT

Params	*Settings*	*Params*	*Settings*
$R_1(k\Omega)$	1	$R_7(k\Omega)$	15
$R_2(k\Omega)$	3	$R_8(k\Omega)$	20
$R_3(k\Omega)$	5	$R_9(k\Omega)$	30
$R_4(k\Omega)$	8	$R_{10}(k\Omega)$	40
$R_5(k\Omega)$	10	$R_{11}(k\Omega)$	500
$R_6(k\Omega)$	12	$C(mF)$	0.1

IV. ENTIRE MEMRISTIVE CIRCUIT DESIGN AND SIMULATION RESULTS OF C. ELEGANS

In this work, a bionic circuit design utilized the general operational amplifier (Fig. 15) based on the locomotion

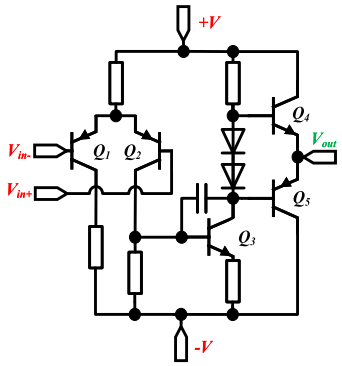

Fig. 15. General operational amplifier schematic.

TABLE III

PARAMETERS OF THE VOLTAGE SIGNALS IN MEMRISTIVE BIONIC C. ELEGANS CIRCUIT

$Params$	$V_{-}(mV)$	$V_{+}(mV)$	$TD(ms)$	$PW(ms)$	$PER(ms)$
V_1	-100	100	0	50	100
V_2	0	38	0	100	100
V_3	100	100	0	100	100
V_{reset}	-0.01	0	0	50	100
V_{reset1}	-50	0	70	2	100
V_b	0	1000	0	100	100

TABLE IV

HARDWARE AREA AND POWER CONSUMPTION OF THE MEMRISTIVE BIONIC CIRCUIT OF C. ELEGANS

Meristive circuit	**Hardware area**	**Power consumption**
Resistance[1]	549 mm^2	9.26 mW
Capacitance[2]	63 mm^2	3.1 uW
Operational amplifier[3]	2850 mm^2	12.71 mW
Total	3462 mm^2	21.97 mW

[1] Hardware area of each resistance is 4.5 mm^2.
[2] Hardware area of each capacitance is 9 mm^2.
[3] Hardware area of each operational amplifier is 50 mm^2 and the schematic is as shown in Fig. 15.

mechanism of C. elegans is proposed, as shown in Fig. 16. The sensory, interneuron, and motoneuron modules detailed in the early sections are integrated to build the C. elegans neural network at the circuit level. The sensory neuron module is comprised of four stimulus sensor circuits (AVM, ALM, PLM, and PVM) to receive and process sensations of anterior or posterior stimulus. It is noted that the connections between neurons manifest two kinds of effects: excitatory (red line) and inhibitory (green line). The interneuron module includes four information processors (AVD, AVA, AVD, and PVC). The interneuron module is a circuit coupler, which allows information from multiple neurons to be gathered together and establish a neural network hierarchy. The Motoneuron module consists of two motion control circuits (A and B) to generate the spiking pulse and a coordinated control circuit (D) to balance A and B. In addition, V_{Ap} and V_{Bp} show the occurrence of backward and forward motion, respectively.

Simulation results of the proposed circuit are shown in Fig. 17. During the first excitation cycle (0–50 ms), V_{AVD} and V_{AVA} inversely correlated with backward locomotion zigzag grow, while AVD and PVC are kept in a suppressed state (below 0 V). The higher the activity of the interneuron, the greater and faster the memristance changes, for instance, M_{AVD} reaches the highest memristance of 22.2 kΩ. Between 0 and 100 ms, V_A reaches the first peak (34 mV) yet is still below the M_A's threshold (38 mV), thus no spiking signals are generated (V_{Apin} and V_{Ap} remain at 0 V). During the second excitation cycle (100–150 ms), V_A increases gradually at point G (24 mV), and then reaches the second peak (42 mV) which is larger than M_A's threshold (38 mV). M_A drops significantly at point C (145 ms), and V_{Apin} starts to rise after decay (5 ms). Between 150 and 171 ms, V_p generates a spiking pulse with the amplitude of 1 V for 21 ms. Once V_A is less than the M_A's threshold at point B, M_A starts to return to the initial state (LRS) and then waits for the next excitation.

V. ROBOTIC APPLICATION

A. Serpentine Robot Based on Modular Design

Snakes not only walk through holes, avoid obstacles, cross deserts, and swim in water but also move rapidly on flat ground in a unique way of high movement efficiency. Researchers in biomimetic mechanics have imitated the movement of snakes and developed a snake-like robot with a large number of degrees of freedom. However, there are still some shortcomings, such as fewer motion modes, complicated control, high quality, low degree of freedom, low sensitivity, and low flexibility between joints. These problems affect the motion efficiency of the snake-like robot, leading to an increase in the failure rate in real-world applications.

As shown in Fig. 18, this section proposes a serpentine robot based on a modular design, which includes three core modules. First, the function of the neuron processor module which receives and processes stimulus is similar to Fig. 16. In general, the skeleton of a biological snake is composed of hundreds of spine bones, and we assume that the number of the spine is equal to n in this work. In addition, the muscular system of C. elegans consists of four quadrants of striated muscles, each of which includes two rows of muscle cells standing side by side, this is, V_A (V_B) and D_A (D_B) represent the ventral motoneuron and dorsal motoneuron of C. elegans, respectively. With further simplification, $A_i (i = 1, 2, 3, \ldots, n)$ represents the joint names. When the wave propagates from the tail of the body to the head, C. elegans is going to crawl backward. Conversely, when the wave spreads from the head to the tail of the body, C. elegans moves forward and $B_i (i = 1, 2, 3, \ldots, n)$ is the joint name of the serpentine robot. Second, in the spiking output module, $V_{\mathrm{Api}}/V_{\mathrm{Bpi}} (i = 1, 2, 3, \ldots, n)$ is the spiking voltage of the i_{th} joint in backward/forward locomotion. At last, the serpentine robot module can utilize these signals, including V_{Api} and $V_{\mathrm{Apin}i}$ (V_{Bpi} and $V_{\mathrm{Bpin}i}$) to design strategies and promote locomotion.

This section considers the backward movement of C. elegans when the frontal stimulus is received. Thus, V_A is generated by motoneuron A. The number of the spine of the serpentine robot is $n = 3$, and simulation results for the spiking output module are shown in Fig. 19. At 68 ms, V_A exceeds the M_{A1}'s threshold, and then M_{A1} drops significantly to around 1 kΩ. After a few microseconds, M_{A2} and M_{A3} decrease

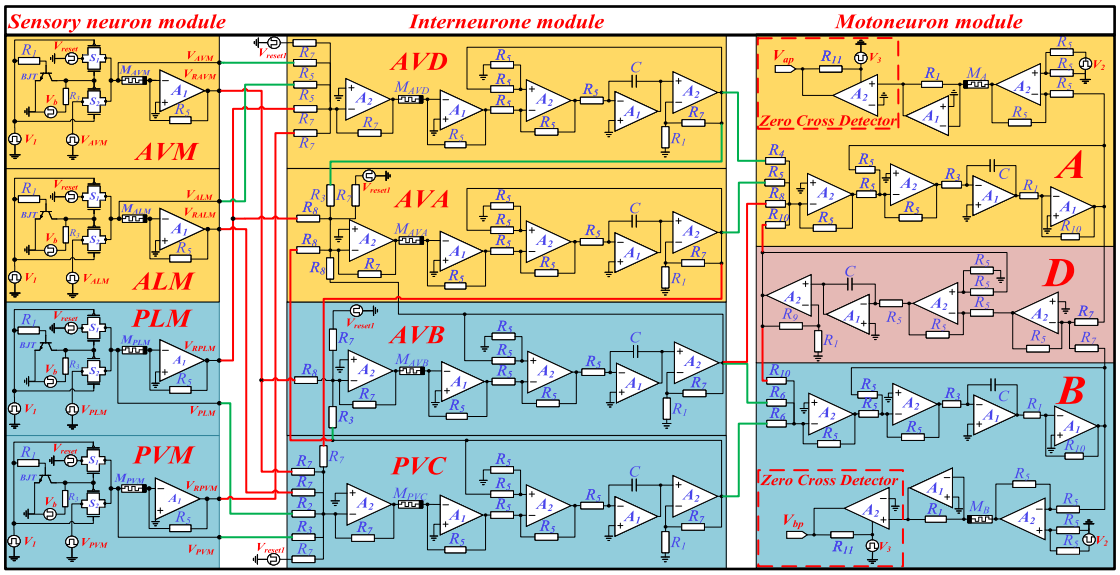

Fig. 16. General diagram of the memristive bionic C. elegans circuit. The green and red connection lines indicate the excitatory and inhibitory effects between two modules, respectively. The parameters of the C. elegans neural circuit are shown in Table II. The parameters of the voltage signals in C. elegans neural circuit are shown in Table III. The power consumption of the circuit is obtained from a PSpice simulation, as shown in Table IV.

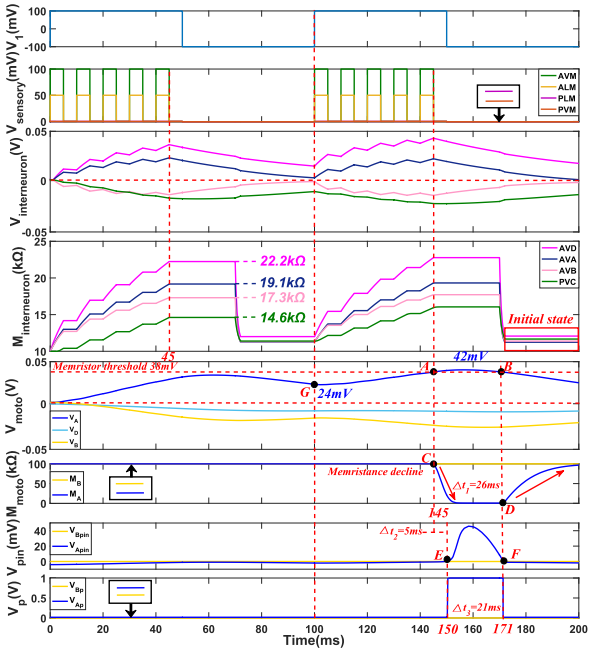

Fig. 17. Circuit simulation results of the memristive bionic C. elegans circuit. The amplitudes of V_{AVM} and V_{ALM} are 0.05 and 0.1 V, respectively, and they have the same duty cycles (50%). The amplitudes of V_{PLM} and V_{PVM} maintain 0 V, which is regarded as not receiving the posterior stimulus.

almost at the same time, and V_{Apin1}, V_{Apin2}, and V_{Apin3} increase to 13.7, 24.2, and 48.5 mV, respectively. It is noted that these three voltages (V_{Apin1}, V_{Apin2}, and V_{Apin3}) show mathematical relations—V_{Apin2} is twice as much as V_{Apin1}, and V_{Apin3} is twice as much as V_{Apin2}. In addition, if we increase the number of serpentine robot spine n, $V_{\mathrm{Apin}n}$ increases exponentially. The above-mentioned discussion presents a quantitative logic—if we know the voltage V_{Apin1} of the first spine, we can infer the voltage $V_{\mathrm{Apin}i}$ of the i_{th} spine and check whether it is wrong.

B. Comparison With Previous Work

Table V compares the works of C. elegans circuit and robot locomotion works in recent years. Using a bidirectional associative memory mechanism and a restricted Boltzmann machine, Raj et al. [49] proposed a new architecture to associate the joint trajectories of humanoid walking and extract the features from trajectories, respectively. This architecture can be applied to the stable walking of humanoid robots in real-time scenarios. Its simulation has been validated with NaO and HOAP2 bioed robots. Berri et al. [50] and Boyle et al. [56] research on how the neurons and muscle of C. elegans create the sinusoid wave and spread from head to tail. Semwal et al. [52], [53] utilized a multilayered ANN to achieve human gait identification with high recognition accuracy, which can be utilized in the detection of age, race, and gender. Furthermore, they also applied DNN models to different walking activities classification. The work enables the generation of the robot walking trajectories. Agarwal et al. [53] utilized a simplified neural network to demonstrate the bionic circuit (CMOS circuit) responsible for touch-induced motion.

The CMOS circuits are limited to fixed-point operations with poor flexibility. Since most of the training uses floating-point operations, the CMOS-based circuits only carrying out fixed-point operations cannot meet the requirements for training. In addition, most of the C. elegans circuits implemented on CMOS cannot implement neuromorphic computing algorithms efficiently, since the CMOS is not designed for brain-inspired analog computing, which further limits improvements of large-scale bionic neural networks in terms of stackability, energy efficiency, and low latency.

To overcome the above-mentioned drawbacks, we propose the neuromemristive circuit to illustrate the locomotion behavior of C. elegans at the circuit level, which provides a new way to hardware implement neuromorphic computing. In particular, the memristor-based C. elegans circuit possesses robust and stable performance. The proposed circuit for the C. elegans locomotion mechanism is different from traditional motion schemes based on basic electric elements. It has a smaller area overhead and is robust to any delay in the stimulation of C. elegans locomotion. Indeed, hardware coupled with a

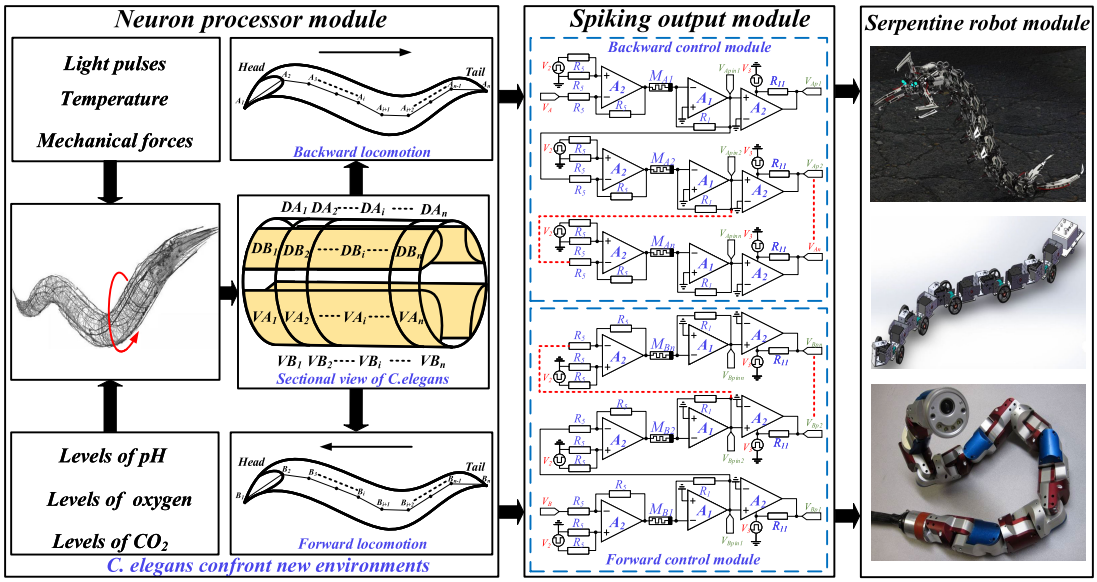

Fig. 18. Schematic of serpentine robot design based on the memristive bionic circuit of C. elegans. The serpentine robot design includes three parts. (a) Neuron processor module. (b) Spiking output module. (c) Serpentine robot module.

TABLE V

COMPARISON BETWEEN THE PROPOSED MEMRISTIVE BIONIC CIRCUIT AND OTHER HARDWARE-BASED C. ELEGANS CIRCUIT

Model	M. Raj [49]	J. H. Boyle [50]	V. B. Semwal [51, 52]	N. Agarwal [53]	Proposed circuit
Method	BAM[1] + RBM[2]	Physics simulator	ANN	Locomotor network	C. elegans
Signal form	Analog signals	Digital signals	Analog signals	Analog signals	Analog signals
Robustness	High	Low	High	Low	High
Simulation	NaO and HOAP2 biped robots	Matlab	Google colab	BioRC circuit library[55]	PSpice
Hardware implementation	No	No	No	Yes	Yes
Biological inspiration	No	Yes	No	Yes	Yes

[1] BAM is bidirectional associative memory.
[2] RBM is restricted Boltzmann machine.

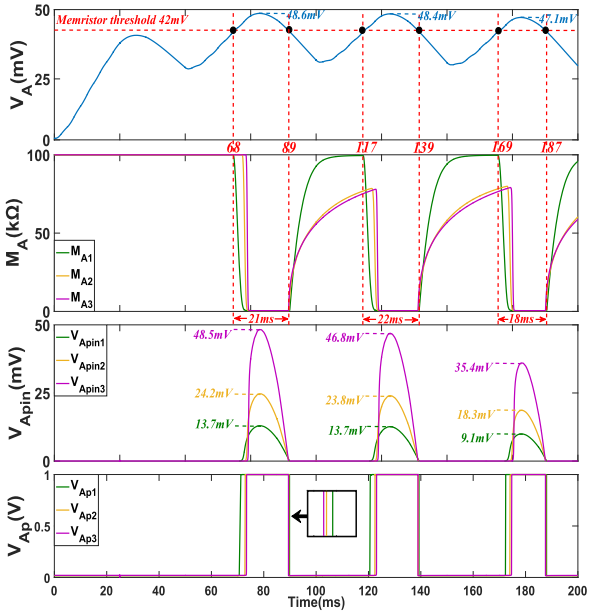

Fig. 19. Simulation results of serpentine robot design based on the memristive circuit of C. elegans.

bionic algorithm could better meet the requirements of high precision, low energy consumption, and low latency. With the simulation and analysis in PSpice, the proposed circuit shows good flexibility; that is, the rate, the duty cycle, and the amplitude of input signals can be adjusted via the circuit parameters while maintaining accuracy having sufficient floating-point performance and effectively improving the utilization of the hardware area.

VI. CONCLUSION

In this article, we propose a novel neuromorphic computing architecture, the serpentine robot system, comprising a multilayer bio-inspired neural network with the LIF-based C. elegans neuron model. The C. elegans neuron model integrates all inputs from neighboring neurons and fires (memristance change) if the sum of inputs reaches the threshold. A biological neural network made of such neurons has been developed, consisting of three layers, including the sensory, interneuron, and motoneuron modules. Importantly, this architecture possesses advantages, such as decent efficiency, robustness, flexibility, and bio-compatibility, which are corroborated by the simulation results. Therefore, our work presents a glimpse of how the hardware implementation of biological neural systems will empower next-generation neuromorphic computing. In the future, we are going to extend our bio-circuit

design toward a larger scale system, which could be integrated with machine learning techniques, aiming to address more complicated tasks.

REFERENCES

[1] J. Grollier, D. Querlioz, and M. D. Stiles, "Spintronic nanodevices for bioinspired computing," *Proc. IEEE*, vol. 104, no. 10, pp. 2024–2039, Oct. 2016.

[2] S. Yu, "Neuro-inspired computing with emerging nonvolatile memory," *Proc. IEEE*, vol. 106, no. 2, pp. 260–285, Feb. 2018.

[3] B. Cramer et al., "Surrogate gradients for analog neuromorphic computing," *Proc. Nat. Acad. Sci. USA*, vol. 119, no. 4, Jan. 2022, Art. no. e2109194119.

[4] X. Liu et al., "Harmonica: A framework of heterogeneous computing systems with memristor-based neuromorphic computing accelerators," *IEEE Trans. Circuits Syst. I, Reg. Papers*, vol. 63, no. 5, pp. 617–628, May 2016.

[5] A. Balaji et al., "Mapping spiking neural networks to neuromorphic hardware," *IEEE Trans. Very Large Scale Integr. (VLSI) Syst.*, vol. 28, no. 1, pp. 76–86, Jan. 2019.

[6] G. Chen et al., "Toward brain-inspired learning with the neuromorphic snake-like robot and the neurorobotic platform," *IEEE Trans. Cognit. Develop. Syst.*, vol. 11, no. 1, pp. 1–12, Mar. 2019.

[7] E. Falotico et al., "Connecting artificial brains to robots in a comprehensive simulation framework: The neurorobotics platform," *Frontiers Neurorobot.*, vol. 11, pp. 1–2, Jan. 2017.

[8] Z. Jiang, Z. Bing, K. Huang, and A. Knoll, "Retina-based pipe-like object tracking implemented through spiking neural network on a snake robot," *Frontiers Neurorobot.*, vol. 13, p. 29, May 2019.

[9] H. Marvi et al., "Sidewinding with minimal slip: Snake and robot ascent of sandy slopes," *Science*, vol. 346, no. 6206, pp. 224–229, Oct. 2014.

[10] F. Sanfilippo, J. Azpiazu, G. Marafioti, A. A. Transeth, O. Stavdahl, and P. Liljeback, "A review on perception-driven obstacle-aided locomotion for snake robots," in *Proc. 14th Int. Conf. Control, Autom., Robot. Vis. (ICARCV)*, Phuket, Thailand, Nov. 2016, pp. 1–7.

[11] F. Sanfilippo, O. Stavdahl, G. Marafioti, A. A. Transeth, and P. Liljeback, "Virtual functional segmentation of snake robots for perception-driven obstacle-aided locomotion?" in *Proc. IEEE Int. Conf. Robot. Biomimetics (ROBIO)*, Qingdao, China, Dec. 2016, pp. 1845–1851.

[12] F. Sanfilippo, O. Stavdahl, and P. Liljeback, "SnakeSIM: A ROS-based rapid-prototyping framework for perception-driven obstacle-aided locomotion of snake robots," in *Proc. IEEE Int. Conf. Robot. Biomimetics (ROBIO)*, Dec. 2017, pp. 1226–1231.

[13] F. Sanfilippo, E. Helgerud, P. A. Stadheim, and S. L. Aronsen, "Serpens, a low-cost snake robot with series elastic torque-controlled actuators and a screw-less assembly mechanism," in *Proc. 5th Int. Conf. Control, Autom. Robot. (ICCAR)*, Apr. 2019, pp. 133–139.

[14] A. Rezaei, Y. Shekofteh, M. Kamrani, A. Fallah, and F. Barazandeh, "Design and control of a snake robot according to snake anatomy," in *Proc. Int. Conf. Comput. Commun. Eng.*, May 2008, pp. 191–194.

[15] R. Ariizumi and F. Matsuno, "Dynamic analysis of three snake robot gaits," *IEEE Trans. Robot.*, vol. 33, no. 5, pp. 1075–1087, Oct. 2017.

[16] N. A. Dunn, J. S. Conery, and S. R. Lockery, "A neural network model for chemotaxis in *Caenorhabditis elegans*," in *Proc. Int. Joint Conf. Neural Netw.*, Jul. 2003, pp. 2574–2578.

[17] J. X. Xu, D. Xin, and D. Ji, "Study on *C. elegans* behaviors using recurent neural network model," in *Proc. IEEE Conf. Cybern. Intell. Syst.*, Jul. 2010, pp. 1–6.

[18] K. Sakamoto, Z. Soh, M. Suzuki, Y. Kurita, and T. Tsuji, "A neural network model of *Caenorhabditis elegans* and simulation of chemotaxis-related information processing in the neural network," in *Proc. SAI Intell. Syst. Conf. (IntelliSys)*, Nov. 2015, pp. 668–673.

[19] X. Deng, Q. Ren, Y. Du, G. Wang, R. Wu, and X. Si, "Modeling the undulatory locomotion of *C. elegans* based on the proprioceptive mechanism," in *Proc. IEEE 23rd Int. Symp. Ind. Electron. (ISIE)*, Jun. 2014, pp. 1560–1565.

[20] Z. Li, J. Li, S. Zhao, Y. Yuan, Y. Kang, and C. Chen, "Adaptive neural control of a kinematically redundant exoskeleton robot using brain–machine interfaces," *IEEE Trans. Neural Netw. Learn. Syst.*, vol. 30, no. 12, pp. 3558–3571, Dec. 2019.

[21] M. Thor and P. Manoonpong, "Error-based learning mechanism for fast online adaptation in robot motor control," *IEEE Trans. Neural Netw. Learn. Syst.*, vol. 31, no. 6, pp. 2042–2051, Jun. 2020.

[22] S. Ma and N. Tadokoro, "Analysis of creeping locomotion of a snake-like robot on a slope," *Auto. Robots*, vol. 20, no. 1, pp. 15–23, Jan. 2006.

[23] A. Crespi, A. J. A. Ijspeert, and E. Polytechnique, "AmphiBot II: An amphibious snake robot that crawls and swims using a central pattern generator," *Color Res. Appl.*, vol. 27, no. 2, pp. 130–135, 2006.

[24] J. Karbowski, G. Schindelman, C. J. Cronin, A. Seah, and P. W. Sternberg, "Systems level circuit model of *C. elegans* undulatory locomotion: Mathematical modeling and molecular genetics," *J. Comput. Neurosci.*, vol. 24, no. 3, pp. 253–276, Jun. 2008.

[25] Q. Ren, X. Deng, and J. Xu, "Generation undulatory locomotion of *C. elegans* in a crawling robot via biomimetic learning," in *Proc. 12th IEEE Int. Conf. Control Autom. (ICCA)*, Jun. 2016, pp. 593–598.

[26] R. Jain, V. B. Semwal, and P. Kaushik, "Deep ensemble learning approach for lower extremity activities recognition using wearable sensors," *Expert Syst.*, vol. 39, no. 6, Jul. 2022, Art. no. e12743.

[27] V. Bijalwan, V. B. Semwal, and T. Mandal, "Fusion of multi-sensor-based biomechanical gait analysis using vision and wearable sensor," *IEEE Sensors J.*, vol. 21, no. 13, pp. 14213–14220, Jul. 2021.

[28] V. B. Semwal, S. A. Katiyar, R. Chakraborty, and G. C. Nandi, "Biologically-inspired push recovery capable bipedal locomotion modeling through hybrid automata," *Robot. Auto. Syst.*, vol. 70, pp. 181–190, Aug. 2015.

[29] T. Ibrayev, A. P. James, C. Merkel, and D. Kudithipudi, "A design of HTM spatial pooler for face recognition using memristor-CMOS hybrid circuits," in *Proc. IEEE Int. Symp. Circuits Syst. (ISCAS)*, May 2016, pp. 1254–1257.

[30] Y. Guo, X. Wang, and Z. Zeng, "A compact memristor-CMOS hybrid look-up-table design and potential application in FPGA," *IEEE Trans. Comput.-Aided Design Integr. Circuits Syst.*, vol. 36, no. 12, pp. 2144–2148, Dec. 2017.

[31] Z. I. Mannan, S. P. Adhikari, C. Yang, R. K. Budhathoki, H. Kim, and L. Chua, "Memristive imitation of synaptic transmission and plasticity," *IEEE Trans. Neural Netw. Learn. Syst.*, vol. 31, no. 10, pp. 3458–3470, Nov. 2019.

[32] J. Chen, Z. Zeng, and P. Jiang, "Global Mittag–Leffler stability and synchronization of memristor-based fractional-order neural networks," *Neural Netw.*, vol. 51, pp. 1–8, Mar. 2014.

[33] D. Querlioz, O. Bichler, and C. Gamrat, "Simulation of a memristor-based spiking neural network immune to device variations," in *Proc. Int. Joint Conf. Neural Netw.*, Jul. 2018, pp. 1775–1781.

[34] Q. Hong, H. Chen, J. Sun, and C. Wang, "Memristive circuit implementation of a self-repairing network based on biological astrocytes in robot application," *IEEE Trans. Neural Netw. Learn. Syst.*, vol. 33, no. 5, pp. 2106–2120, May 2022.

[35] H. Lin and C. Wang, "Influences of electromagnetic radiation distribution on chaotic dynamics of a neural network," *Appl. Math. Comput.*, vol. 369, Mar. 2020, Art. no. 124840.

[36] M. Chalfie, J. E. Sulston, J. G. White, E. Southgate, J. N. Thomson, and S. Brenner, "The neural circuit for touch sensitivity in *Caenorhabditis elegans*," *J. Neurosci.*, vol. 5, no. 4, pp. 956–964, Apr. 1985.

[37] L. Emtage, G. Gu, E. Hartwieg, and M. Chalfie, "Extracellular proteins organize the mechanosensory channel complex in *C. elegans* touch receptor neurons," *Neuron*, vol. 44, no. 5, pp. 795–807, Dec. 2004.

[38] L. R. Girard et al., "WormBook: The online review of *Caenorhabditis elegans* biology," *Nucleic Acids Res.*, vol. 35, pp. D472–D475, Jan. 2007.

[39] P. D. Mcclanahan, J. H. Xu, and F. Y. Christopher, "Comparing *Caenorhabditis elegans* gentle and harsh touch response behavior using a multiplexed hydraulic microfluidic device," *Integrative Biol.*, vol. 9, no. 10, 2017, Art. no. 1744806917707667.

[40] A. L. Nekimken, B. L. Pruitt, and M. B. Goodman, "Touch-induced mechanical strain in somatosensory neurons is independent of extracellular matrix mutations in *C. elegans*," *Mol. Biol. Cell*, vol. 31, no. 16, pp. 1735–1743, 2020.

[41] W. Li, Z. Feng, P. W. Sternberg, and X. Z. Shawn Xu, "A *C. elegans* stretch receptor neuron revealed by a mechanosensitive TRP channel homologue," *Nature*, vol. 440, no. 7084, pp. 684–687, Mar. 2006.

[42] J.-X. Xu and X. Deng, "Complex chemotaxis behaviors of *C. elegans* with speed regulation achieved by dynamic neural networks," in *Proc. Int. Joint Conf. Neural Netw. (IJCNN)*, Jun. 2012, pp. 1–8.

[43] J. Joshi, C. C. Hsu, A. C. Parker, and P. Deshmukh, "A carbon nanotube cortical neuron with excitatory and inhibitory dendritic computations," in *Proc. Life Sci. Syst. Appl. Workshop*, 2009, pp. 133–136.

[44] S. Gao, M. Zhou, Y. Wang, J. Cheng, H. Yachi, and J. Wang, "Dendritic neuron model with effective learning algorithms for classification, approximation, and prediction," *IEEE Trans. Neural Netw. Learn. Syst.*, vol. 30, no. 2, pp. 601–614, Feb. 2018.

[45] Y. Zhang, X. Wang, Y. Li, and E. G. Friedman, "Memristive model for synaptic circuits," *IEEE Trans. Circuits Syst. II, Exp. Briefs*, vol. 64, no. 7, pp. 767–771, Jul. 2017.

[46] M. A. Nahmias, B. J. Shastri, A. N. Tait, and P. R. Prucnal, "A leaky integrate-and-fire laser neuron for ultrafast cognitive computing," *IEEE J. Sel. Top. Quantum Electron.*, vol. 19, no. 5, pp. 1–12, Sep. 2013.

[47] J.-K. Han et al., "Mimicry of excitatory and inhibitory artificial neuron with leaky integrate-and-fire function by a single MOSFET," *IEEE Electron Device Lett.*, vol. 41, no. 2, pp. 208–211, Feb. 2020.

[48] F. Kiani, J. Yin, Z. Wang, J. J. Yang, and Q. Xia, "A fully hardware-based memristive multilayer neural network," *Sci. Adv.*, vol. 7, no. 48, Nov. 2021, eabj4801.

[49] M. Raj, V. B. Semwal, and G. C. Nandi, "Bidirectional association of joint angle trajectories for humanoid locomotion: The restricted Boltzmann machine approach," *Neural Comput. Appl.*, vol. 30, no. 6, pp. 1747–1755, Sep. 2018.

[50] S. Berri, J. H. Boyle, M. Tassieri, I. A. Hope, and N. Cohen, "Forward locomotion of the nematode *C. Elegansis* achieved through modulation of a single gait," *HFSP J.*, vol. 3, no. 3, pp. 186–193, Jun. 2009.

[51] V. B. Semwal, N. Gaud, P. Lalwani, V. Bijalwan, and A. K. Alok, "Pattern identification of different human joints for different human walking styles using inertial measurement unit (IMU) sensor," *Artif. Intell. Rev.*, vol. 55, no. 2, pp. 1149–1169, Feb. 2022.

[52] V. B. Semwal, M. Raj, and G. C. Nandi, "Biometric gait identification based on a multilayer perceptron," *Robot. Auto. Syst.*, vol. 65, pp. 65–75, Mar. 2015.

[53] N. Agarwal, N. Mehta, A. C. Parker, and K. Ashouri, "*C. elegans* neuromorphic neural network exhibiting undulating locomotion," in *Proc. Int. Joint Conf. Neural Netw. (IJCNN)*, May 2017, pp. 3912–3921.

[54] Y. Irizarry-Valle and A. C. Parker, "Astrocyte on neuronal phase synchrony in CMOS," in *Proc. IEEE Int. Symp. Circuits Syst. (ISCAS)*, Jun. 2014, pp. 261–264.

[55] J. H. Boyle and N. Cohen, "*Caenorhabditis elegans* body wall muscles are simple actuators," *Biosystems*, vol. 94, nos. 1–2, pp. 170–181, Oct. 2008.

[56] J. H. Boyle, S. Berri, and N. Cohen, "Gait modulation in *C. elegans*: An integrated neuromechanical model," *Frontiers Comput. Neurosci.*, vol. 6, p. 10, Mar. 2012.

Hegan Chen received the B.S. degree from the College of Computer Science and Electronic Engineering, Hunan University, Hunan, in 2021. He is currently pursuing the M.Phil. degree with the Department of Electrical and Electronic Engineering, The University of Hong Kong, Hong Kong.

His current research interests include memristors and their applications to machine learning.

Qinghui Hong received the B.S. and M.S. degrees in electronic science and technology from Xiangtan University, Xiangtan, China, in 2012 and 2015, respectively, and the Ph.D. degree in computer system architecture from the Huazhong University of Science and Technology, Wuhan, China, in 2019.

He is currently an Associate Professor with the College of Computer Science and Electronic Engineering, Hunan University, Changsha, China. He has authored or coauthored more than 30 Science Citation Index (SCI) papers, including the IEEE TRANSACTIONS ON NEURAL NETWORKS AND LEARNING SYSTEMS, IEEE TRANSACTIONS ON BIOMEDICAL CIRCUITS AND SYSTEMS (TBCS), IEEE TRANSACTIONS ON COMPUTER-AIDED DESIGN OF INTEGRATED CIRCUITS AND SYSTEM (TCAD), IEEE TRANSACTIONS ON VERY LARGE SCALE INTEGRATION SYSTEMS (TVLSI), and IEEE TRANSACTIONS ON CIRCUITS AND SYSTEMS (TCAS)—I. His current research interests include memristive neural networks, brain-like computing circuits, and their applications to artificial intelligence.

Zhongrui Wang received the B.Eng. degree (Hons.) and the Ph.D. degree from the Nanyang Technological University, Singapore, in 2009 and 2014, respectively.

He was a Post-Doctoral Research with the University of Massachusetts Amherst, Amherst, MA, USA. He is currently an Assistant Professor with the Department of Electrical and Electronic Engineering, The University of Hong Kong, Hong Kong. His research interests include emerging memory-based neuromorphic computing, machine learning, and modeling memristive materials using density functional theory.

Chunhua Wang received the M.S. degree from Zhengzhou University, Zhengzhou, China, in 1994, and the Ph.D. degree from Beijing University of Technology, Beijing, China, in 2003.

He is currently a Professor with the College of Information Science and Engineering, Hunan University, Changsha, China, where he is also a Doctor Tutor and the Director of the Advanced Communication Technology Key Laboratory, Hunan University. He has presided over eight national and provincial projects. He has authored or coauthored more than 120 papers, among which more than 100 were retrieved by Science Citation Index (SCI). His research interests include memristor circuits, complex networks, chaotic circuits, chaos secure communication, current-mode circuits, and neural networks based on memristors.

Dr. Wang is a member of the Academic Committee of Hunan University and the Director of the Chaos and Nonlinear Circuit Professional Committee of the Circuit and System Branch, China Electronic Society.

Xiangxiang Zeng (Senior Member, IEEE) received the Ph.D. degree in system engineering from the Huazhong University of Science and Technology, Wuhan, China, in 2011.

He was with the Department of Computer Science, Xiamen University, Xiamen, China. In 2019, he joined Hunan University, Changsha, China, where he is currently a Yuelu Distinguished Professor with the College of Information Science and Engineering. He was a Visiting Scholar with Oklahoma State University, Stillwater, OK, USA, and the Harvard Medical School, Boston, MA, USA. He has authored or coauthored over 100 articles in journals and conferences. His current research interests include computational intelligence, graph neural networks, and bioinformatics.

Dr. Zeng has over 4000 Google Scholar citations.

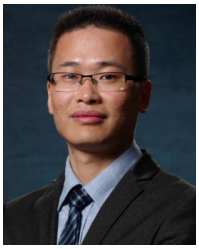

Jiliang Zhang (Senior Member, IEEE) received the Ph.D. degree in computer science and technology from Hunan University, Changsha, China, in 2015.

From 2013 to 2014, he was a Research Scholar with the Maryland Embedded Systems and Hardware Security Laboratory, University of Maryland, College Park, MD, USA. From 2015 to 2017, he was an Associate Professor with Northeastern University, Shenyang, China. He is currently a Full Professor with Hunan University, where he is also the Director of the Chip Security Institute. He has authored more than 60 technical papers in leading journals and conferences. His current research interests include hardware security, integrated circuit designs, and intelligent systems.

Dr. Zhang is the Secretary General of the CCF Fault-Tolerant Computing Professional Committee. He was a recipient of the CCF Integrated Circuit Early Career Award. He is serving as a Steering Member for the Hardware Security Forum of China and a Guest Editor for the IEEE TRANSACTIONS ON CIRCUITS AND SYSTEMS (TCAS) II: Express Briefs.